Geometrically frustrated $GdInO_3$: An exotic system to study negative thermal expansion and spin-lattice coupling

Barnita Paul, Swastika Chatterjee, and Anushree Roy*
Department of Physics, Indian Institute of Technology Kharagpur 721302, India

A. Midya and P. Mandal†
Saha Institute of Nuclear Physics, Homi Bhabha National Institute, 1/AF Bidhannagar, Calcutta 700 064, India

Vinita Grover and A. K. Tyagi
Chemistry Division, Bhabha Atomic Research Centre, Mumbai 400085, India

(Received 20 August 2016; revised manuscript received 16 January 2017; published 6 February 2017)

In this article, we report negative thermal expansion and spin frustration in hexagonal $GdInO_3$. Rietveld refinements of the x-ray diffraction patterns reveal that the negative thermal expansion in the temperature range of 50–100 K stems from the triangular lattice of Gd^{3+} ions. The downward deviation of the low-temperature inverse susceptibility (χ^{-1}) versus T plot from the Curie-Weiss law and the large value of the ratio, $|\theta_{CW}|/T_N > 28$, where θ_{CW} and T_N are respectively Curie-Weiss and Neel temperature, indicate a strong spin frustration, which inhibits long-range magnetic ordering down to 1.8 K. Magnetostriction measurements clearly demonstrate a spin-lattice coupling in the system. Low-temperature anomalous phonon softening, as obtained from temperature-dependent Raman measurements, also reveals the same. Our experimental observations are supported by first-principles density functional theory calculations of the electronic and phonon dispersion in $GdInO_3$. The calculations suggest that the $GdInO_3$ lattice is highly frustrated at low temperature. Further, the calculated normal mode frequencies of the Gd-related Γ point phonon modes reveal significant magnetoelastic coupling in this system. The competitive role of magnetic interaction energy and thermal stabilization energy in determining the change in interatomic distances is the possible origin for the negative thermal expansion in $GdInO_3$ over a limited range of temperature.

DOI: 10.1103/PhysRevB.95.054103

I. INTRODUCTION

In recent years, RTO_3-type (R = rare-earth, T = transition metal) rare-earth ferrites, manganites, or nickelates found special interest due to their multiferroic characteristics [1–6]. The role of d-shell electrons of T ions, governing the multiferroic properties of these systems, has been explored extensively. Unlike the above materials, if T belongs to a nontransition metal ion, the electric or magnetic properties of the system are expected to arise only from the $4f$-shell electrons of the rare-earth ion R. In this regard, rare-earth indates, $RInO_3$, have emerged as potential candidates for fascinating ferroelectric memory devices [7–10]. The noncentrosymmetric atomic arrangement in the hexagonal unit cell of this system gives rise to the geometric ferroelectricity [11]. Among all compounds in the rare-earth indate series, $GdInO_3$ draws a special attention because of the presence of Gd^{3+} ion, which has exact half-filled $4f$ shell as the outermost orbital. The Gd^{3+} ion shows pure spin magnetism with $\vec{L} = 0$, $\vec{J} = \vec{S} = 7/2$. Due to the isotropic g factor, specifying the magnetic moment of Gd^{3+}, one expects $GdInO_3$ as a classical Heisenberg system. Furthermore, in the literature we find that some of the Gd-based compounds exhibit negative thermal expansion (NTE). While the mechanism of NTE in crystalline Gd [14] is associated with the change in magnetic ordering, the same is attributed to the transverse vibrational motion of the two-coordinated Pd atom in $GdPd_3B_{0.25}C_{0.75}$ [15]. This indicates the origin of NTE to depend on the crystalline environment of Gd ions in a system. Along with large spontaneous polarization [11], the possibility of the appearance of the above-discussed features marks $GdInO_3$ as an exotic system. Although In^{3+} does not play any direct role on spin ordering in $GdInO_3$, the noncentrosymmetric distortion in the crystal structure due to the large In^{3+} ion is expected to yield a complex interplay between spin and lattice degrees of freedom in this system.

In the present work, we discuss the magnetic ordering, the crystal structure, and the possibility of spin and lattice coupling in the $GdInO_3$ compound. We have observed NTE in this system over the temperature range between 50 and 100 K. The role of Gd^{3+} ions for NTE is evident from the Rietveld refinement of low-temperature x-ray diffraction (XRD) patterns. In addition, the spin frustration in this system is confirmed from the temperature dependence of the magnetic susceptibility. Low-temperature magnetostriction measurements indicate the coupling between spin and lattice in $GdInO_3$. The anomalous softening of the phonon mode in the low-temperature range also reveals the same. Experimental observation has been further supported by the first-principles density functional theory (DFT) calculations of the electronic and phonon dispersion in $GdInO_3$. Our calculations reveal that the lattice is highly frustrated and there does exist a substantial amount of spin-lattice coupling in this system. The present article is organized as follows. In Sec. II, we discuss the experimental and computational details. Section III presents

*anushree@phy.iitkgp.ernet.in
†prabhat.mandal@saha.ac.in

the results regarding NTE and spin frustration in $GdInO_3$. After which the spin-lattice coupling in this system is discussed. Finally, in Sec. IV we summarize our results.

II. EXPERIMENTAL AND COMPUTATIONAL DETAILS

The bulk powder of $GdInO_3$ was prepared by the self-assisted gel combustion method. The stoichiometric amount of Gd_2O_3 and In_2O_3 were dissolved in nitric acid followed by the addition of glycine. Glycine acts as a fuel and also as a complexing agent. A gel was formed by evaporating the solution at the temperature of 80–100° C. It was then heated up to 250° C. The obtained powder was calcined at 550° C for 1 h and then annealed at 850° C for 12 h. The details of the synthesis procedure are reported elsewhere [11].

Rietveld refinement of the XRD patterns were carried out using FULLPROF software [12]. DIAMOND 4.0 crystallography software [13] was used to obtain the interatomic distances in the refined structure. Raman measurements were carried out using a micro-Raman spectrometer (TRIAX550, JY, France), equipped with a Peltier-cooled charge coupled device (CCD) as the detector (Synapse, JY, Horiba). A laser irradiation of 488-nm wavelength with 3-mW laser power was used as an excitation source to avoid the heating of the sample. A 50L× microscope objective was used for focusing the light on the sample. Temperature variation was carried out using a sample stage and a temperature controller along with a liquid nitrogen pump (THMS-600, Linkam, UK) over the temperature range 78 to 300 K. From 300 to 240 K, spectra were recorded at a temperature interval of 15 K whereas at 10 K interval over the range of 230–180 K and 5 K interval for 175–78 K.

Magnetization measurements down to 1.8 K were carried out using SQUID VSM (Quantum Design) and heat capacity was measured in a physical properties measurement system (Quantum Design). We have measured the change in the length of the sample over the temperature range of 5–300 K by the capacitive method using a miniature tilted-plate dilatometer. The capacitance has been measured by an Andeen Hagerling 2700A Ultra-precision Capacity Bridge. In this technique, a change in the sample length can be measured very accurately [16]. The absolute resolution of this measurement is about 1 Å. The room temperature and zero field dimension of our sample was 1 mm × 1 mm ×1 mm. The longitudinal magnetostriction was measured with field applied parallel to the sample length.

First-principles calculations were performed within the framework of density functional theory (DFT) [17,18] using the projector augmented wave (PAW) [19,20] method as implemented in the plane-wave based VASP code [21–23]. The exchange-correlation functional was chosen to be the Perdew-Burke-Ernzerhof (PBE) [24] implementation of the generalized gradient approximation (GGA). An energy cutoff of 450 eV was used for plane wave expansions. To include the strong correlation effects of *4f* electrons of Gd, we used the spin-polarized GGA plus Hubbard U (GGA + U) [25] method, as in the Dudarev's implementation [26], with $U - J = 4.6$ eV [27]. The ionic positions as well as the lattice parameters have been relaxed using a conjugate-gradient algorithm, until the Helmann-Feynman forces become less than 0.005 eV/Å. The energy convergence with respect to the computational parameters was carefully examined. The Γ point phonon frequencies have been calculated using the density functional perturbation theory (DFPT) [28] as implemented in the VASP code.

III. RESULTS AND DISCUSSION

A. Structural anomaly and spin-frustration in $GdInO_3$

Figure 1 displays the coupling of temperature with lattice degrees of freedom in $GdInO_3$ by plotting the relative thermal expansion of the sample length (L), defined by $\frac{\Delta L}{L(0)} \equiv \frac{L(T)-L(0)}{L(0)}$, over the temperature range between 5 and 300 K. $L(0)$ is the length of the sample at 5 K (the lowest temperature down to which the measurement was carried out). Below room temperature, the plot exhibits expected monotonic decreasing trend till 100 K. Between 100 and 50 K, the value of ΔL increases with the decrease in temperature, followed by a smooth downturn upon further lowering of the temperature. The increase in ΔL with lowering of temperature, over the range between 50 and 100 K, indicates NTE of the system in this range of temperature. Since we have used polycrystalline $GdInO_3$ sample for our study, at each temperature the value of $\Delta L/L$ in Fig. 1 corresponds to the averaged value [29,30] of the same in all three crystallographic axes of the compound.

To decipher the origin of NTE, as seen in Fig. 1, we probe the effect of temperature on the crystal structure of $GdInO_3$. Figure 2 shows the powder XRD patterns of the compound at 50, 100, and 300 K. Rietveld refined patterns are shown by the red solid lines in the figure. All patterns could be fitted with noncentrosymmetric $P6_3cm$ space group. This rules out the possibility of any structural phase transition to be the origin of NTE, observed in Fig. 1, in the temperature range between 50 and 100 K. Figure 3(a) plots the lattice parameters, a, c, and unit cell volume (V) at three temperatures, as obtained from the Rietveld analysis of the diffraction data. We find that the decrease in unit cell volume with the decrease in temperature from 300 to 100 K, determined from the XRD data [Fig. 3(a)], is ∼0.6%. In contrast, the decrease in volume of the sample over this temperature range, as could be estimated from the dilatometry measurement, is ∼0.3%. As in dilatometry we followed high precision measurements, the discrepancy in the estimated fractional change in volume by two techniques, may be due to the fact that the actual experimental errors in

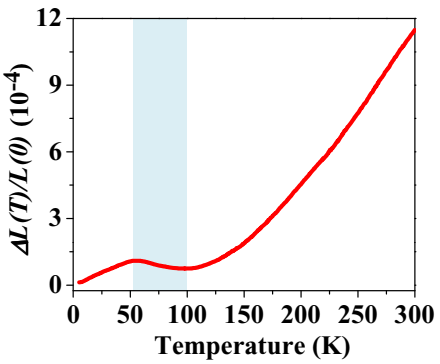

FIG. 1. Temperature dependence of the relative length change $\Delta L/L(0)$. Blue shaded zone marks the temperature range for negative thermal expansion.

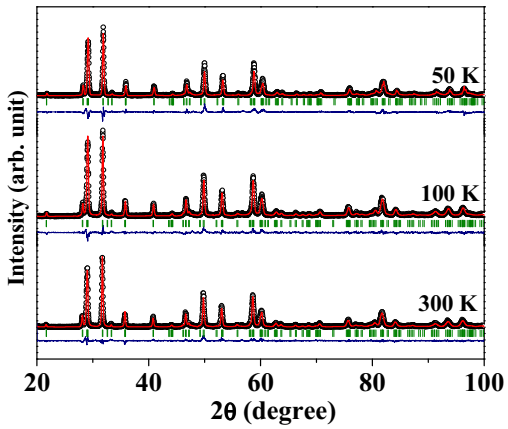

FIG. 2. Rietveld refined pattern of $GdInO_3$ at 50, 100, and 300 K. The red lines are the fitted patterns. The green bars show the positions of Bragg reflection peaks and the blue lines are the difference between the experimental and calculated patterns in each panel.

the values of the cell parameters [Fig. 3(a)] are higher than the statistical standard deviation, obtained from the Rietveld analysis of the XRD data. It is to be noted from Fig. 1 that for $GdInO_3$, in the temperature range 100–50 K, the linear thermal expansion coefficient α_L is $\sim 6 \times 10^{-7}$ K^{-1}. Thus, it is nontrivial to find the reflection of the expected small change in lattice parameters in the XRD pattern over the temperature range between 50 and 100 K. Therefore, instead of analyzing the change in lattice parameters, we carefully examined interatomic distances in the refined structure. It is to be noted that this may reveal the contribution of a specific atomic plane in anomalous structural distortion for NTE.

The atomic arrangement of a hexagonal $GdInO_3$ unit cell with noncentrosymmetric $P6_3cm$ space group is shown in

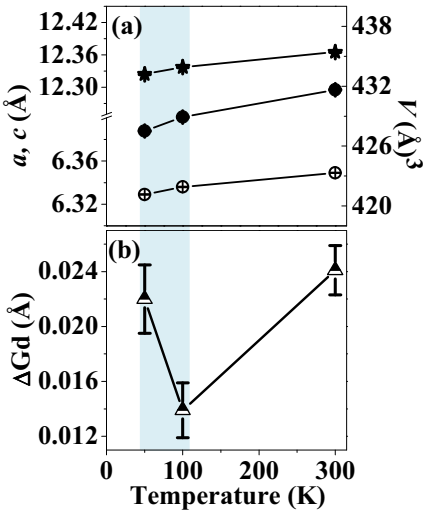

FIG. 3. (a) Variation in $a(\circ)$, $c(*)$, and cell volume $(V,\bullet)$ with temperature. The standard deviation of the refined parameters, as obtained from Rietveld analysis, are shown as error bars. The error bars are within the size of the symbols. (b) Variation of $(\Delta Gd = d_1 - d_2)$ with temperature. The added standard deviations of d_1 and d_2 are shown as the error bars for each data point.

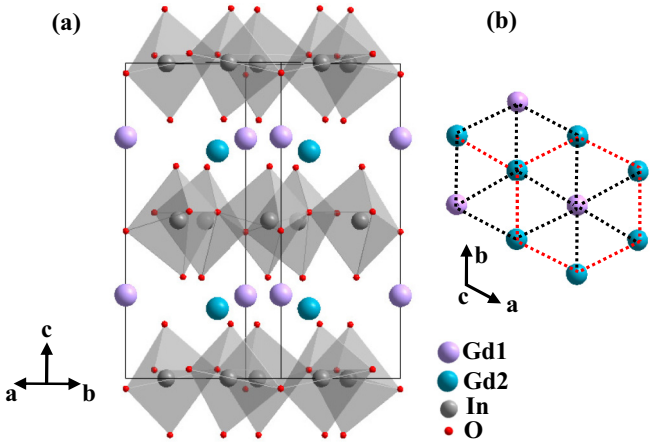

FIG. 4. (a) Crystal structure of hexagonal $GdInO_3$ and (b) triangular arrangement of Gd ions viewed along c-axis.

Fig. 4(a). Gd1 and Gd2 are two inequivalent Gd atoms with Wyckoff positions 2a and 4b, respectively. The hexagonal structure consists of tilted InO_5 bipyramids with two apical (O1, O2) and three planar oxygen ions (O3, O4, O4). Two inequivalent atomic positions of Gd ions form a triangular lattice, as shown in Fig. 4(b), between two InO_5 bipyramidal layers. Two different arm lengths, $d_1 = \text{Gd1} - \text{Gd2}$ (black dashed lines) and $d_2 = \text{Gd2} - \text{Gd2}$ (red dashed lines), are involved in forming the triangular lattice. Interestingly, we find that the difference between these two distances, $(\Delta Gd = d_1 - d_2)$, does not change monotonically with temperature, as shown in Fig. 3(b). At 300 K, the difference is 0.024 Å, which is 0.014 Å at 100 K. The difference again increases to 0.022 Å at 50 K. Comparing Fig. 1 and Fig. 3(b) it appears that the above anomalous lattice distortion in the Gd plane is reflected in NTE of $GdInO_3$ over the temperature range between 50 and 100 K. For a single crystal of $GdInO_3$, the difference in thermal expansion along the a and c axes of the unit cell is expected to reveal the above-discussed anomalous behavior of the Gd plane over the temperature range between 50 and 100 K. For hexagonal $HoMnO_3$, a similar study has been exploited to investigate the origin of NTE in this system [31]. For our polycrystalline sample, as mentioned earlier, the dilatometry measurement yields only the averaged value of the thermal expansion. Thus, at this point we refrain from commenting more on the origin of NTE in $GdInO_3$ from this particular measurement.

To explore the magnetic behavior, we have carried out magnetization measurements at constant temperature ($M - H$ plot at 2 K) and at constant field ($M - T$ plot at 50 Oe), Figs. 5(a) and 5(b), respectively. From Fig. 5 (a) it is clear that $M(H)$ does not show any field-induced metamagnetic transition as observed in several rare-earth transition metal oxides. At low-field and low-temperature (2 K), M increases approximately linearly with field and a downward curvature appears in the high field region, but no clear saturation is observed up to 7 T. With increasing temperature, M is observed to decrease rapidly and $M(H)$ becomes almost linear up to 7 T [refer to the inset of Fig. 5 (a)]. However, the presence of a short-range magnetically ordered phase was identified from the temperature dependence of the inverse

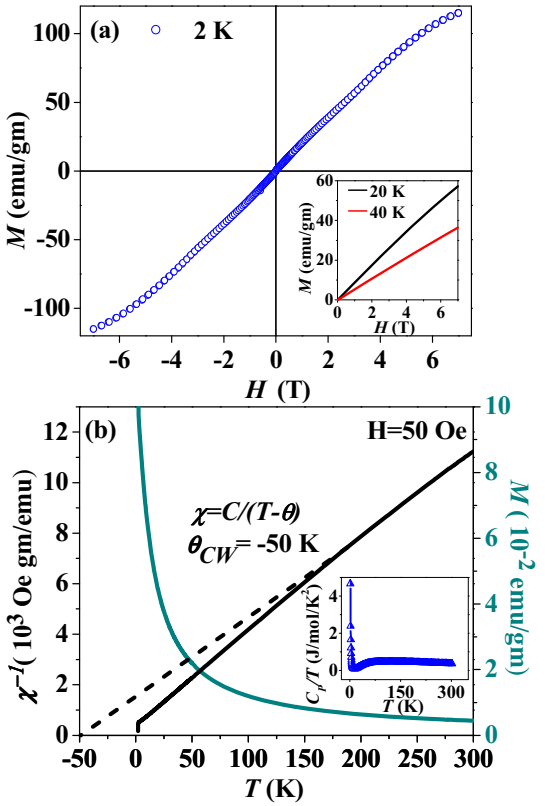

FIG. 5. (a) $M-H$ curve at 2 K. Inset of the figure shows the first quadrant $M-H$ plots at 20 K and 40 K, (b) $M-T$ and $\chi^{-1}-T$ plots at H=50 Oe(green and black solid lines, respectively). The dashed line corresponds to the Curie-Weiss law. Inset of the figure shows C_p/T vs T plot.

susceptibility χ^{-1} $(=H/M)$ plot, shown by the black solid line in Fig. 5(b). Though the susceptibility follows the Curie-Weiss-like behavior at high temperature, it shows a deviation from the linearity below 150 K (the dashed line marks the expected Curie-Weiss linear plot). The extrapolated Curie-Weiss temperature ($\theta_{\rm CW}$) is found to be -50 K. It is to be noted that χ^{-1} versus T plotted in Fig. 5(b) shows a sharp drop just below 1.8 K. The inset of Fig. 5(b) plots the variation of specific heat with temperature (C_p/T versus T). We observe a sharp upturn of the plot just below 1.8 K. The sharp changes in heat capacity and magnetization indicate the onset of antiferromagnetic ordering just below 1.8 K.

Below 150 K, the deviation of the χ^{-1} versus T plot [Fig. 5(b)] from the linearity of the Curie-Weiss behavior indicates a strong spin fluctuation in the paramagnetic phase of the system. Several hexagonal rare-earth transition metal oxides with chemical formula RTO_3 (where $R=$ Gd, Tb, Dy, . . . ,Lu and $T=$ Mn, Fe, Cr) exhibit spin fluctuation due to geometrical frustration as a result of nearly triangular networks. Despite strong antiferromagnetic interaction, the long-range ordering of the magnetic ions in these compounds can be found at much lower temperature (T_N) than the Curie-Weiss temperature $|\theta_{\rm CW}|$ (magnetic energy scale, derived from the bulk susceptibility). The reduction in Neel temperature, T_N, is a signature of spin fluctuations due to the geometrical frustration. The ratio $|\theta_{\rm CW}|/T_N$ can be used as a measure of

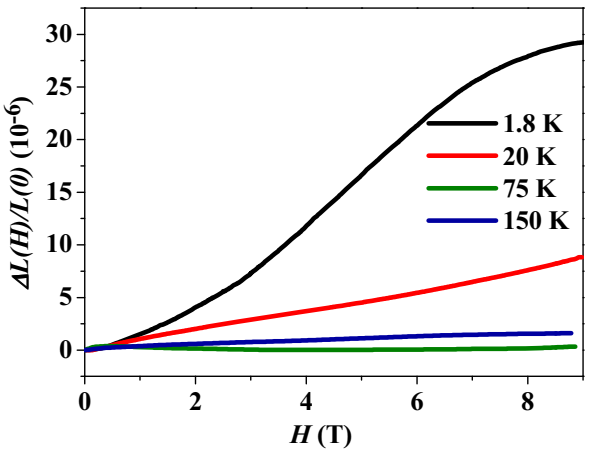

FIG. 6. Magnetostriction plotted as $\Delta L(H)/L(0)$ vs. H at 1.8, 20, 75, and 150 K.

the spin frustration strength [32–35]. If this ratio is larger than 10, the spin system is classified as the one with strong geometrical frustration since such a huge reduction in T_N cannot be explained by the simple mean-field theory [34]. In well-known hexagonal manganites, the maximum value of $|\theta_{\rm CW}|/T_N$ is reported to be 10 for $R=$ Lu and Y. It is to be noted that these are considered as strongly frustrated systems [32–35]. As mentioned above, in $GdInO_3$ there is an onset of antiferromagnetic ordering below 1.8 K. From the susceptibility data we find $|\theta_{\rm CW}|/T_N > 28$, which is about three times larger than the value reported for the hexagonal manganites. Thus, we believe that $GdInO_3$ is a strongly spin frustrated system like other multiferroics.

B. Spin-lattice coupling in $GdInO_3$

In the above discussion, we confirm the presence of a short-range magnetic ordering in $GdInO_3$ over a wide range of temperature. The antiferromagnetic ordering in the system is expected only below 1.8 K. A magnetostriction measurement is often used to study the strength of coupling between spin and lattice. $\Delta L(H)/L(0) \equiv [L(H)-L(0)]/L(0)$ plots, recorded at 1.8, 20, 75, and 150 K, are shown in Fig. 6. $L(0)$ is the sample length at zero field. At 1.8 K, $\Delta L(H)/L(0)$ exhibits a change in slope at $\sim$3 T and starts to level off above 6 T. It is to be noted that without any coupling between the spin and lattice, one expects that $\Delta L(H)/L(0)$ should be close to zero and independent of the applied magnetic field. Moreover, the observed behavior of $\Delta L(H)/L(0)$ is quite similar to $M(H)$ at 2 K. The above result is a clear indication of the coupling of lattice and spin degrees of freedom in $GdInO_3$.

With an increase in temperature, the value of $\Delta L(H)/L(0)$ decreases rapidly. The weakening of magnetoelastic coupling with an increase in T is expected because of the strong decrease of magnetization with temperature as shown in the inset of Fig. 5(a). Interestingly, we observe that the slope is less for the plot recorded at 75 K than the same at 150 K. It is to be recalled that the temperature 75 K lies within the range of NTE and 150 K lies well above it [refer to Fig. 1]. We believe that upon the onset of spin frustration near 150 K, the interatomic distances in the triangular lattice of magnetic

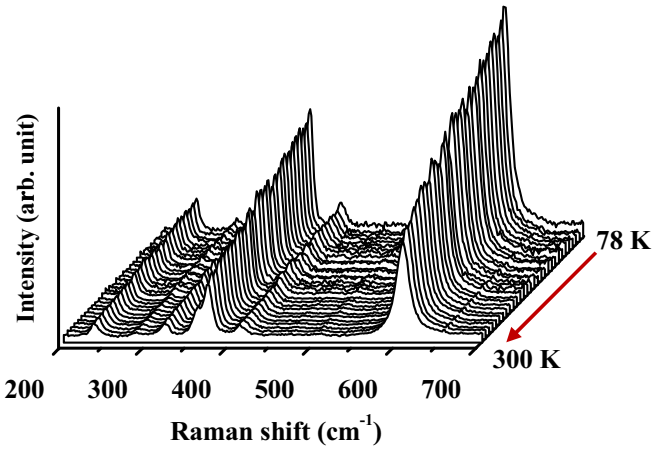

FIG. 7. Temperature-dependent Raman spectra of $GdInO_3$ in the spectral range of 200 to 700 cm^{-1} after linear baseline correction.

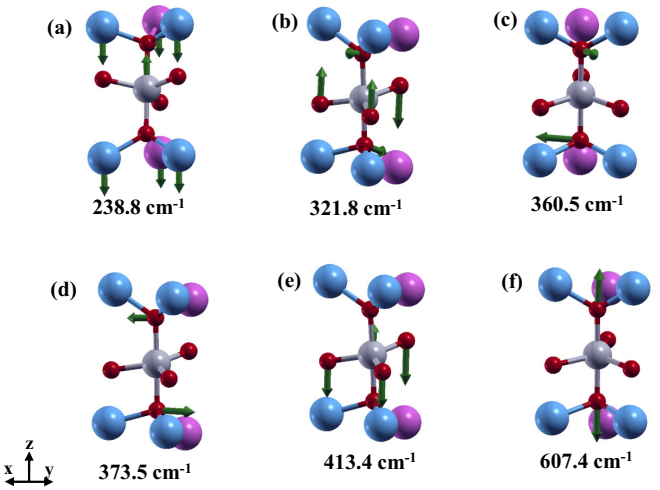

FIG. 8. Calculated atomic displacement patterns for experimentally observed Raman modes involving Gd1 (magenta spheres), Gd2 (blue spheres), In (grey spheres), and O (red spheres). The experimental values of the corresponding phonon wave numbers at room temperature are available in each panel. The green arrows mark the directions of the vibration of the atoms involved.

Gd^{3+} ion fail to contract to the values expected due to thermal stabilization only, resulting in a flattening of the $\Delta L/L(0)$ plot just below 150 K in Fig. 1. Near 75 K the competition between thermal and spin energies results in anomalous behavior of the magnetostriction plot. It will be interesting to probe the correlation between spin and thermal expansivity along the *a* and *c* axes of the single crystalline $GdInO_3$ lattice, as for such a system the magnetic correlation is expected to be different in these two directions. Here we would like to mention that, in the literature, NTE due to coupling between the magnetic order and thermal stabilization of the magnetic ions, and hence the complex behavior of magnetostriction plot, has been discussed in hexagonal manganites and chromates systems [31,36]. Our results, in a way, confirm our earlier claim on the role of magnetic Gd ions in governing the NTE in $GdInO_3$.

Furthermore, the possibility of the coupling between the spin and lattice degrees of freedom has been probed by temperature-dependent Raman measurements over the range between 78 and 300 K and is shown in Fig. 7 (after a linear background subtraction). All spectra were recorded over the spectral range of 200–700 cm^{-1}. Each spectrum in Fig. 7 was deconvoluted by seven Lorentzian profiles, keeping peak position, width, and intensity of all peaks as free fitting parameters.

We consider only the prominent Raman modes at around ~239, 322, 361, 374, 413, and 607 cm^{-1} for further discussion. The atomic vibrations corresponding to these modes are discussed in detail in our earlier report [11]. From the calculated phonon density of states [11] the assignments of the observed modes were obtained theoretically by studying atomic displacements related to closest computed mode frequencies for $GdInO_3$. Figure 8 schematically shows the atomic displacements related to each measured Raman wave number.

The deconvolution of Raman spectra (after a linear background subtraction) by seven Lorentzian profiles provides us the evolution of the Raman shift for all modes over the given range of temperature. Figure 9 plots the variation of the peak positions for the above-mentioned modes (shown by symbols) with temperature, as obtained from the deconvolution of the spectra. The corresponding atomic vibrations of all Raman modes from Ref. [11] are mentioned in each panel of Fig. 9. The change in Raman shift with temperature at a constant pressure only due to thermal anharmonicity can be expressed as follows [37,38]:

$$\left(\frac{d\omega}{dT}\right)_P = \left(\frac{\partial\omega}{\partial T}\right)_V + \left(\frac{\partial\omega}{\partial V}\right)_T \left(\frac{\partial V}{\partial T}\right)_P. \quad (1)$$

Using the following definitions of Grüneisen parameter (γ) and volume thermal expansion coefficient (α_V),

$$\gamma = -\frac{\partial(ln\omega)}{\partial(lnV)};\ \alpha_V = \frac{1}{V}\left(\frac{\partial V}{\partial T}\right), \quad (2)$$

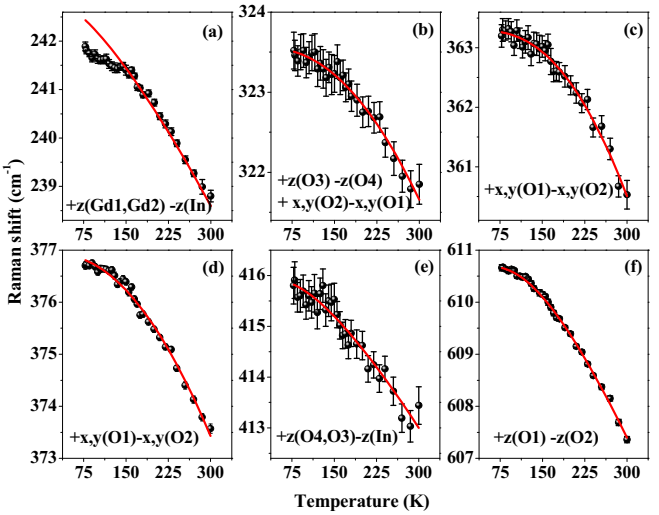

FIG. 9. Evolution of Raman modes (mentioned in the text) with temperature for $GdInO_3$.

Eq. (1) becomes

$$\frac{1}{\omega}\left(\frac{d\omega}{dT}\right)_P = \frac{1}{\omega}\left(\frac{\partial\omega}{\partial T}\right)_V - \gamma\alpha_V. \quad (3)$$

The first term in the right-hand side (R.H.S) of Eq. (3) represents the true anharmonic contribution of the temperature on the mode frequency due to the anharmonic potential. The second term represents the change in the frequency due to the change in cell volume with temperature. In our case, the thermal expansion coefficient $\alpha_V \approx 3\alpha_L$ is only $\sim 10^{-6}$ (refer to Fig. 1), and hence the contribution of volume contraction on the change in the frequency of the phonon modes with lowering of temperature can be neglected. Thus, in Fig. 9 we analyze the experimentally obtained data points only by considering the true anharmonic contribution of temperature on the phonon frequency. The solid red lines are generated by taking into account the four-phonon decay process due to the increase in anharmonicity in the vibrational potential with temperature [39] by following the relations

$$\omega_{anh} = \omega_0 + \Delta(T), \quad (4)$$

$$\Delta(T) = A\left(1 + \frac{2}{(e^{\phi/2} - 1)}\right) + B\left(1 + \frac{3}{(e^{\phi/3} - 1)} + \frac{3}{(e^{\phi/3} - 1)^2}\right),$$

where ω_0 is the phonon frequency at 0 K, $\phi = \hbar\omega_0/k_B T$ and A and B are anharmonic constants.

We find that data points for all modes, except the one at $\sim$239 cm^{-1} could be fitted by a set of constants A, B, and ω_0 for each, for the whole range of temperature between 78 and 300 K [see the red solid lines in Figs. 9(b) to 9(f)]. The clear change in the slope of the observed phonon frequency of the Raman mode at $\sim$239 cm^{-1} near 150 K compelled us to fit the data points with free fitting parameters up to 150 K using Eq. (4) [refer to the red solid line in the panel (a) of Fig. 9]. The deviation of the measured frequency of the Raman mode near 239 cm^{-1} from the expected anharmonic frequency (solid line) indicates an additional factor to be responsible for the anomalous shift. The atomic vibrations related to the Raman mode at 239 cm^{-1} involve the vibration of Gd^{3+} and In^{3+} ions along the c axis, and is shown in the Fig. 8(a). It is to be noted that this is the only mode under study which involves the vibration of Gd ions. The absence of such an anomaly in other Raman modes [Figs. 9(b) to 9(f)], confirms the role of the magnetic Gd plane as the origin of the anomalous phonon softening and indicates the magnetoelastic coupling in this system. Here we would like to mention that the higher deviation of experimental data points from the expected plot due to thermal anharmonicity in Fig. 9(a) indicates higher spin-lattice coupling at 75 K than at 150 K. This contradicts our experimental finding from magnetostriction measurements in Fig. 6, where the opposite trend is observed. This can be justified by the fact mentioned above: The anomaly in small change in volume of the crystal near NTE region, as measured in Fig. 1, is not expected to be reflected in the shift in Raman measurements.

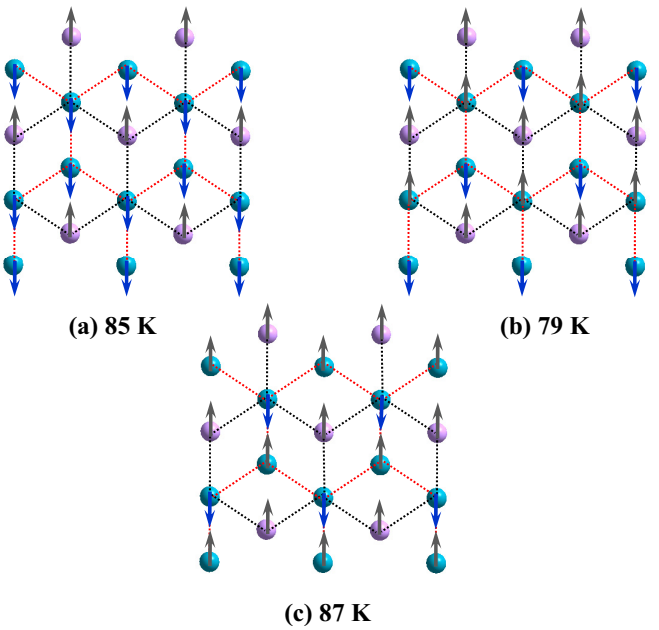

FIG. 10. Schematic diagram of all AFM configurations in Gd triangular lattice. The relative stabilization energy of different AFM configurations with respect to the FM configuration has been indicated at the bottom of each AFM configuration.

The interplay between the spin and lattice degrees of freedom in $GdInO_3$ was further investigated using first-principles calculations. The $GdInO_3$ lattice was fully optimized, starting from the room temperature experimental data. To determine the preferred magnetic orientation of Gd, we performed total energy calculations for all possible magnetic configurations of Gd in the $GdInO_3$ lattice. If one considers the $P6_3cm$ symmetry group of $GdInO_3$, there are only three possible AFM magnetic configurations of the Gd triangular lattice, as shown in Fig. 10. We find that all antiferromagnetic configurations are energetically very close, the difference being of the order of 0.001 eV ($\sim$ 10 K), but they are lower than the ferromagnetic

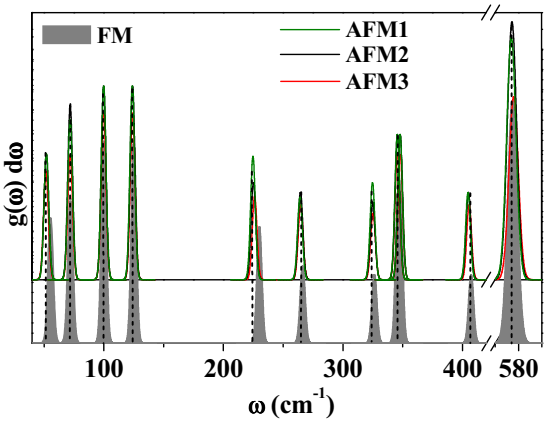

FIG. 11. Calculated phonon spectra of $GdInO_3$ for FM (shown by the filled area) and all three AFM (shown by the solid line) configurations at 0 K. Dashed lines mark the shift in phonon wave numbers between two magnetic states.

TABLE I. Calculated phonon wavenumbers over the range between 50 cm^{-1} and 600 cm^{-1} in all magnetic configurations. $\Delta = \frac{\omega_{AFM}-\omega_{FM}}{\omega_{FM}} \times 100\%$ for all three AFM configurations 1, 2, and 3 are listed in sequence.

Magnetic States	Calculated phonon modes, ω in cm^{-1}										
AFM1	52.1	72.3	100	124.1	224.9	264.3	324.8	345.7	347.9	404.7	577.98
AFM2	52.1	72.1	100.1	124.1	225.3	264.6	325.0	345.7	348.0	405.1	577.25
AFM3	52.7	72.2	100.1	124.3	226.3	264.8	325.3	345.7	348.1	405.7	577.99
FM	55.7	72.5	100.4	125.0	230.1	266.1	326.3	346.1	348.8	407.2	578.96
Δ	− 6.46	− 0.27	− 0.39	− 0.72	− 2.26	− 0.67	− 0.46	− 0.11	− 0.26	− 0.61	− 0.34
	− 6.46	− 0.55	− 0.29	− 0.72	− 2.09	− 0.56	− 0.39	− 0.11	− 0.23	− 0.51	− 0.29
	− 5.38	− 0.41	0.29	− 0.56	− 1.65	− 0.49	− 0.30	− 0.11	− 0.20	− 0.37	− 0.17

(FM) configuration by ∼0.01 eV. This clearly suggests that at 0 K the $GdInO_3$ lattice is highly frustrated. An evidence of frustration is also obtained, where we observe a decrease in the ΔGd upon lowering of temperature. The estimated value of ΔGd is 0.04 Å at 300 K and only 0.02 Å at 0 K, as obtained from *ab initio* calculations. The change is very small.

We also studied the change in the phonon frequencies with change in the magnetic ordering of the Gd^{3+} ions in $GdInO_3$. For this purpose we calculated the Γ-point phonons for FM ordering of Gd^{3+} ions and all three possible AFM alignments of the Gd^{3+} ions in Fig. 10. The calculated phonon density of states over the range between 50 and 600 cm^{-1} for all magnetic states are shown in Fig. 11 and phonon wave numbers are listed in Table I. In the same table we also list the percentage change (Δ) in phonon wave numbers between AFM and FM states. An examination of the values of Δ for all phonon modes indeed shows a significant softening of Gd-related vibrational modes (compared to others) as we alter the magnetic structure of the lattice. The calculated phonon mode near 230 cm^{-1} (experimentally appeared at 239 cm^{-1}), which involves Gd ions, is found to soften appreciably as we go from FM to AFM configurations. For other modes the change is relatively less. It is to be recalled that experimentally, we observed a significant softening of this phonon mode relative to other phonon modes (refer to Fig. 9). Thus, it is reasonable to conclude that without spin-phonon coupling, the Gd-related phonon mode frequencies would not have been modified so drastically with a change in magnetic ordering of the system as we find experimentally, which is further supported by *ab initio* calculations. Here, we would like to mention that the change in internal positions of Gd1–Gd2 and Gd2–Gd2 in FM and AFM configurations are within 0.2%.

IV. CONCLUSION

To summarize, we demonstrate NTE in hexagonal $GdInO_3$ at the temperature range of 50–100 K. The corresponding change in the crystal structure is manifested in the triangular lattice of Gd^{3+} ions. The onset of spin frustration at 150 K with a large frustration parameter hinders the long-range magnetic ordering in the system. We find an onset of antiferromagnetic ordering only at a very low temperature. Magnetostriction measurement and the anomalous softening of the phonon mode of Gd-related atomic vibration indicate a spin-phonon coupling in this system. Our claims are further supported by first-principles phonon calculations. We also discuss the possibility of a competition between magnetic interaction energy and thermal stabilization energy in determining the change in interatomic distances, which is the possible origin for the negative thermal expansion in $GdInO_3$.

ACKNOWLEDGMENTS

The authors thank Dr. P. U. Sastry, BARC, Mumbai, for low-temperature XRD measurements and Dr. Rakesh Shukla, BARC, Mumbai, for his contribution in sample preparation. A.R. and V.G. thank Board of Research in Nuclear Sciences, Govt. of India for financial assistance. S.C. thanks Department of Science and Technology, Govt. of India for the Inspire fellowship.

[1] Z. J. Huang, Y. Cao, Y. Y. Sun, Y. Y. Xue, and C. W. Chu, Phys. Rev. B **56**, 2623 (1997).
[2] G. Giovannetti, S. Kumar, D. Khomskii, S. Picozzi, and J. van den Brink, Phys. Rev. Lett. **103**, 156401 (2009).
[3] W. Wang, J. Zhao, W. Wang, Z. Gai, N. Balke, M. Chi, H. N. Lee, W. Tian, L. Zhu, X. Cheng, D. J. Keavney, J. Yi, T. Z. Ward, P. C. Snijders, H. M. Christen, W. Wu, J. Shen, and X. Xu, Phys. Rev. Lett. **110**, 237601 (2013).
[4] H. Das, A. L. Wysocki, Y. Geng, W. Wu, and C. J. Fennie, Nat. Commun. **5**, 1 (2014).
[5] C. Xu, Y. Yang, S. Wang, W. Duan, B. Gu, and L. Bellaiche, Phys. Rev. B **89**, 205122 (2014).
[6] A. Paul, P. Sharma, and U. V. Waghmare, Phys. Rev. B **92**, 054106 (2015).
[7] S. C. Abrahams, Acta Crystallogr. Sect. B **57**, 485 (2001).
[8] T. Tohei, H. Moriwake, H. Murata, A. Kuwabara, R. Hashimoto, T. Yamamoto, and I. Tanaka, Phys. Rev. B **79**, 144125 (2009).
[9] R. Shukla, V. Grover, S. K. Deshpande, D. Jain, and A. K. Tyagi, Inorg. Chem. **52**, 13179 (2013).
[10] R. Shukla, F. N. Sayed, V. Grover, S. K. Deshpande, A. Guleria, and A. K. Tyagi, Inorg. Chem. **53**, 10101 (2014).
[11] B. Paul, S. Chatterjee, S. Gop, A. Roy, V. Grover, R. Shukla, and A. K. Tyagi, Mater. Res. Express. **3**, 075703 (2016).

[12] J. Rodríguez-Carvajal, FULLPROF version 1.6, A Program for Rietveld refinement and pattern matching analysis, avaialable at https://www.ill.eu/sites/fullprof/.
[13] H. Putz, and K. Brandenburg, Diamond—Crystal and molecular structure visualization crystal impact, available at http://www.crystalimpact.com/diamond.
[14] Yu. V. Ergin, J. Exp. Theor. Phys. **21**, 709 (1965).
[15] A. Pandey, C. Mazumder, R. Ranganathan, S. Tripathi, D. Pandey, and S. Dattagupta, Appl. Phys. Lett **92**, 261913 (2008).
[16] M. Rotter, H. Müller, E. Gratz, M. Doerr, and M. Loewenhaupt, Rev. Sci. Instrum. **69**, 2742 (1998).
[17] P. Hohenberg and W. Kohn, Phys. Rev. **136**, B864 (1964).
[18] W. Kohn and L. J. Sham, Phys. Rev. **140**, A1133 (1965).
[19] P. E. Blöchl, Phys. Rev. B **50**, 17953 (1994).
[20] G. Kresse and D. Joubert, Phys. Rev. B **59**, 1758 (1999).
[21] G. Kresse and J. Hafner, Phys. Rev. B **47**, 558 (1993).
[22] G. Kresse and J. Furthmüller, Comput. Mater. Sci. **6**, 15 (1996).
[23] G. Kresse and J. Furthmüller, Phys. Rev. B **54**, 11169 (1996).
[24] J. P. Perdew, K. Burke, and M. Ernzerhof, Phys. Rev. Lett. **77**, 3865 (1996).
[25] J. Hubbard, Proc. R. Soc. London A **276**, 238 (1963).
[26] S. L. Dudarev, G. A. Botton, S. Y. Savrasov, C. J. Humphreys, and A. P. Sutton, Phys. Rev. B **57**, 1505 (1998).
[27] M. Topsakal and R. M. Wentzcovitch, Comput. Mater. Sci. **95**, 263 (2014).
[28] S. Baroni, S. de Gironcoli, A. Dal Corso, and P. Giannozzi, Rev. Mod. Phys. **73**, 515 (2001).
[29] J. A. Souza, J. J. Neumeier, B. D. White, and Y. K. Yu, Phys. Rev. B **81**, 172410 (2010).
[30] M. Nandi, N. Khan, D. Bhoi, A. Midya, and P. Mandal, J. Phys. Chem. C **118**, 1668 (2014).
[31] C. dela Cruz, F. Yen, B. Lorenz, Y. Q. Wang, Y. Y. Sun, M. M. Gospodinov, and C. W. Chu, Phys. Rev. B **71**, 060407(R) (2005).
[32] T. J. Sato, S.-H. Lee, T. Katsufuji, M. Masaki, S. Park, J. R. D. Copley, and H. Takagi, Phys. Rev. B **68**, 014432 (2003).
[33] T. Katsufuji, M. Masaki, A. Machida, M. Moritomo, K. Kato, E. Nishibori, M. Takata, M. Sakata, K. Ohoyama, K. Kitazawa, and H. Takagi, Phys. Rev. B **66**, 134434 (2002).
[34] T. Katsufuji, S. Mori, M. Masaki, Y. Moritomo, N. Yamamoto, and H. Takagi, Phys. Rev. B **64**, 104419 (2001).
[35] J. Park, J.-G. Park, G. S. Jeon, H.-Y. Choi, C. Lee, W. Jo, R. Bewley, K. A. McEwen, and T. G. Perring, Phys. Rev. B **68**, 104426 (2003).
[36] S. Kitani, M. Tachibana, N. Taira, and H. Kawaji, Phys. Rev. B **87**, 064402 (2013).
[37] P. S. Peercy and B. Morosin, Phys. Rev. B **7**, 2779 (1973).
[38] T. R. Ravindran, A. K. Arora, and T. A. Mary, Phys. Rev. B **67**, 064301 (2003).
[39] M. Balkanski, R. F. Wallis, and E. Haro, Phys. Rev. B **28**, 1928 (1983).